Review Paper
Int'l J. of Aeronautical & Space Sci. 11(4), 247–265 (2010)
DOI:10.5139/IJASS.2010.11.4.247

IJASS
International Journal of Aeronautical and Space Science

Multi-Objective Design Exploration and its Applications

Shigeru Obayashi*, Shinkyu Jeong* and Koji Shimoyama*

Institute of Fluid Science, Tohoku University, Katahira, Aoba, Sendai, Japan

Kazuhisa Chiba**

Department of Mechanical Systems Engineering, Hokkaido Institute of Technology, Teine, Sapporo, Japan

Hiroyuki Morino***

Mitsubishi Aircraft Corporation, Oye-cho, Minato, Nagoya, Japan

Abstract

Multi-objective design exploration (MODE) and its applications are reviewed as an attempt to utilize numerical simulation in aerospace engineering design. MODE reveals the structure of the design space based on trade-off information. A self-organizing map (SOM) is incorporated into MODE as a visual data mining tool for the design space. SOM divides the design space into clusters with specific design features. This article reviews existing visual data mining techniques applied to engineering problems. Then, we discuss three applications of MODE: multidisciplinary design optimization for a regional-jet wing, silent supersonic technology demonstrator and centrifugal diffusers.

Key words: Multidisciplinary design optimization, Evolutionary computation, Multiobjective optimization, Data mining, Self-organizaing map, Response surface method

1. Introduction

Multidisciplinary design optimization (MDO) is gaining great importance in aerospace engineering. A typical MDO problem involves multiple competing objectives. While single objective problems may have a unique optimal solution, multi-objective problems (MOPs) have a set of compromising solutions, largely known as the trade-off surface, Pareto-optimal solutions or non-dominated solutions. These solutions reveal trade-off information among different objectives. They are optimal in the sense that no other solutions in the search space are superior to them when all objectives are taken into consideration. A designer will be able to choose a final design with further considerations.

Evolutionary algorithms (EAs) (Deb, 2001) are suitable for finding many Pareto-optimal solutions. However, because EAs are population-based approaches, they generally require a large number of function evaluations. To alleviate the computational burden, the use of the response surface method (RSM) has been introduced as a surrogate model (Queipo et al., 2005). The surrogate model used in this study is the Kriging model (Jeong and Obayashi, 2005; Jones et al., 1998; Keane, 2003).

This approach for finding many Pareto solutions operates sufficiently in its present condition; however, smooth operation is achieved only when the number of objectives remains small. To reveal the trade-off information from the resultant Pareto front for real-world problems containing many objectives, visualization of the Pareto front becomes an issue. The next section reviews visual data mining in engineering design.

A MDO system denoted multi-objective design exploration (MODE) was proposed in Obayashi et al. (2005) and is illustrated in Fig. 1. MODE is not intended to provide an optimal solution. MODE reveals the structure of the

ⓒ* Professor, Corresponding author
E-mail: obayashi@ifs.tohoku.ac.jp Tel: +81-22-217-5265

** Associate Professor
*** Assistant Manager

http://ijass.or.kr pISSN: 2093-274x eISSN: 2093-2480

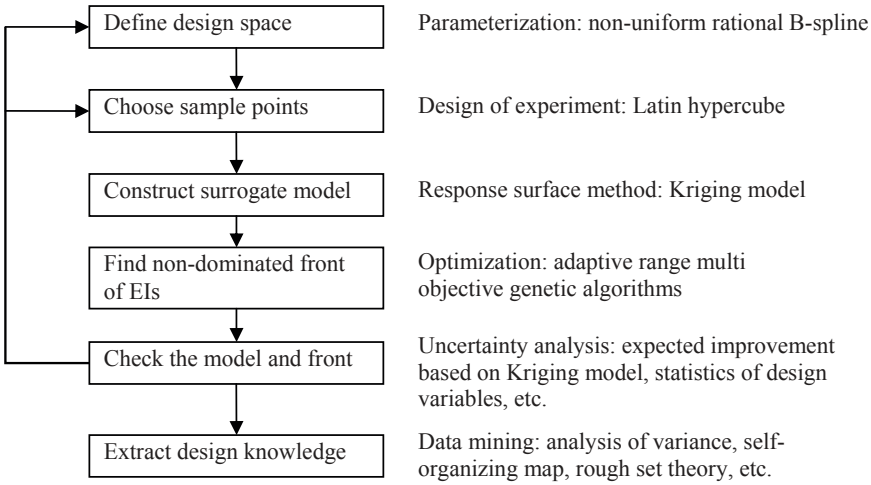

Fig. 1. Flowchart of multi-objective design exploration with component algorithms.

design space from trade-off information and visualizes it as a panorama for a decision maker. The present form of MODE consists of the Kriging model, adaptive range multi objective genetic algorithms, analysis of variance and a self-organizing map (SOM) (Kohonen, 1995). SOM divides the design space into clusters. Each cluster represents a set of designs containing specific design features. A designer may find an interesting cluster with good design features. Such design features are composed of a combination of design variables. If a particular combination of design variables is identified as a sufficient condition belonging to a cluster of interest, it can be considered as a design rule. Rough set theory (Pawlak, 1982) and other data mining techniques have been employed to extract design rules. Through the applications of MODE, this article illustrates the importance of understanding the design problem better instead of obtaining a single optimal solution.

This article reviews existing visual data mining techniques applied to engineering problems. Then, we discuss three applications of MODE: MDO for a regional-jet wing, the silent supersonic technology demonstrator (S3TD) and centrifugal diffusers.

2. Review of Visual Data Mining

2.1 Multi-dimensional multivariate visualization

Wong and Bergeron (1997) reported that "*the main objectives of multi-dimensional multivariate (MDMV) visualization are to visually summarize an MDMV data set, and find key trends and relationships among the variates*." To achieve this goal, extensive research has been conducted in many fields (Alpern and Carter, 1991; Chernoff, 1973; Inselberg, 1997; Inselberg and Dimsdale, 1990; van Wijk and Liere, 1993; Wong and Bergeron, 1997). Among the methods developed to date, parallel coordinates (Inselberg, 1997; Inselberg and Dimsdale, 1990) and the scatter plot matrix are the most widely used approaches in the field of engineering design because of their ease of use. Recently, SOMs (Cios et al., 1998; Deb, 2001) have attracted attention as a novel means for MDMV visualization. The SOM approach entails an unsupervised neural network technique that classifies, organizes, and visualizes large data sets. It projects multidimensional data on a 2-D map without any information loss. In this study, we applied SOM to find the tradeoffs between objective functions, relationships between objective functions, and design variables. Additionally, SOM was employed to determine the sweet spot of the design space (Jeong et al., 2005 a and B; Kumano et al., 2006a; Obayashi et al., 2007). Parashar et al. (2008) used SOM for Pareto solution analysis and decision-making. Generative topographic mapping (GTM) (Svensen, 1998) is another novel MDMV visualization method, which is based on a constrained mixture of Gaussians the parameters which can be optimized using the expectation maximization algorithm. Holden and Keane (2004) used GTM to visualize the high-dimensional data of aircraft design. Pryke et al. (2007) adopted "Heatmaps" to visualize the results of MOP. These novel visualization methods can supply more information than primitive visualization methods. However, users are required to be familiar with reading the results. For visualization of the Pareto frontier of MOP, Mattson and Messac (2003) introduced the s-Pareto Frontier method, and Agrawal et al. (2004) proposed hyper-space diagonal counting (HSDC) and hyperspace Pareto frontier (HPF) (Agrawal et al., 2006).

2.2 Visual design steering

Recent developments have sought to support visual design steering (VDS), which is a modification of the computational steering paradigm (Parker et al., 1997). VDS was first suggested by Winer and Bloebaum (2002a; 2002b) to incorporate the designer's experiences and intuition into the optimization process in order to efficiently obtain an optimum solution. They used graph morphing to show trends in the performance space corresponding to changes in the design variables. In VDS, the designer can stop and change the direction of exploration at any stage during the optimization. Eddy and Lewis (2002) introduced cloud visualization (CV) to support visual steering. In CV, all previously obtained design points are presented as clouds in both the design and performance spaces. These spaces are displayed in separate windows and are linked to each other. A similar visualization system called synchronous visualization (SV) was suggested by Jeong et al. (2007) to visualize parameter subspaces and function space at the same time. Recently, ARL trade space visualizer (ATSV) (Stump et al., 2002, 2004), originally introduced as a graphical user interface tool supporting the "design by shopping" paradigm, has been equipped with the visual steering command (Simpson et al., 2008; Stump et al., 2009) in order to reinforce the trade (or design) space exploration process. VDS linked with high-performance computing and meta-modeling techniques provides the possibility of finding a better solution in complicated system designs using less design time.

Kodiyalam et al. (2004) introduced a rapid method for the visualization of physical model behavior during an optimization run by adopting high-performance computing and surrogate modeling. This method identifies how the responses of the physical model will change with changes in the design variables as optimization is running. Messac and Chen (2000) suggested a method for real-time visualization of the optimization process. The technique for the visualization of the path through the design space of the solutions during evolutionary optimization run was developed by Pohlheim (1999). Ligetti et al. (2003) investigated the impact of graphical interface delay on the efficiency and effectiveness of the design results (Ligetti and Simpson, 2005; Simpson et al., 2005).

2.3 Non-visual data mining

Recently, non-visual data mining techniques have been applied to MDO data to extract specific design rules. The most widely used non-visual data mining method in engineering design is the analysis of variance (ANOVA). ANOVA quantitatively illustrates the effects of each design variable or interaction of design variables of the objective function (Jeong et al., 2005a; Shimoyama et al., 2010). Sugimura et al. (2010) and Graening et al. (2008) introduced decision tree analysis (Witten and Frank, 2005) in order to obtain the design rules and knowledge for a centrifugal impeller and 3-D turbine blade, respectively. Decision tree analysis, developed in the field of statistical science, uses a type of ANOVA to extract design rules that support decision-making. Figure 2 shows a tree diagram obtained by decision tree analysis. By tracing a path to reach a desired node, a single design rule can be obtained. For example, the following if-then type rule can be found by tracing the path represented by the thick line in Fig. 3

$$if\ (dv_1 > a_1)\ \text{and}\ if\ (dv_3 \le a_3)\ and\ ,\ldots\ldots,\ then(P > b_n) \tag{1}$$

where dv_i is the i-th design variable and a_i is the criterion for dividing dv_i. P is performance and b_i is the criterion for dividing the performance P.

Rough set and association rules are additional non-visual data mining methods used to extract design rules. Rough set theory, a mathematical method developed by Pawlak (1982), was originally applied to analyze human senses because how it treats ambiguous data and extracts underlying rules from the data. The concept and procedure for extracting design rules from engineering design data using rough set theory are briefly explained in Fig. 3. In contrast to decision tree theory, multiple design rules are obtained from the rough set theory. To only obtain meaningful rules, rule sets are screened by

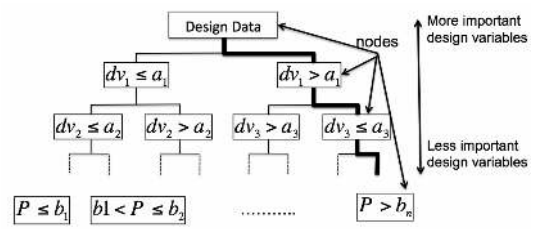

Fig. 2. Diagram of a decision tree.

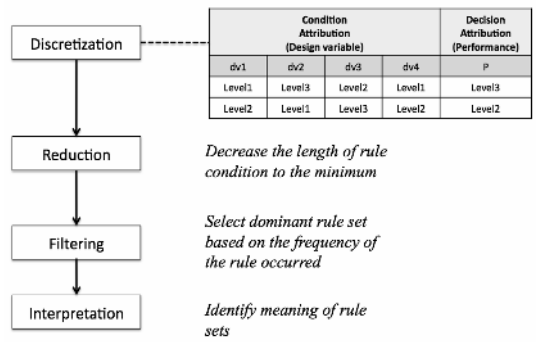

Fig. 3. Procedure for extracting rule sets with the rough set theory.

reduction and filtering. Similar to the rough set theory, the association rule generates many different rules. To select only the important rules, criteria such *as support*, *confidence*, and *lift* are used in the association rule. Sugimura et al. (2009a, b) applied rough set and association rules to obtain the tradeoff rules of a robust centrifugal fan design. Proper orthogonal decomposition (POD), which is known as the principal component analysis in statistical science, has been used to extract dominant features of designed transonic airfoil geometry. In this method, the design data are decomposed into a set of optimum orthogonal base vectors. Subsequently, features of these vectors are investigated in order to extract information. This method has been extended to extraction of the flow field characteristic of a transonic airfoil (Oyama et al., 2010).

3. MDO for the Regional-Jet Wing with Engine-Airframe Integration

In Japan, the New Energy and Industrial Technology Development Organization (NEDO) subsidized the development of an environmentally friendly high performance small jet aircraft. Mitsubishi Heavy Industries, Ltd. (MHI) was the prime contractor for the project. The purpose of this project was to build a prototype aircraft using advanced technologies, such as low-drag wing design, and lightweight composite structures, which were necessary for the reduction of environmental burdens. In March 2008, MHI decided to bring this conceptual aircraft into commercial use. This commercial jet aircraft, named the Mitsubishi regional jet (MRJ), has a capacity of about 70-90 passengers. This project focused on environmental issues, such as reduction of exhaust emissions and noise. Moreover, in order to bring the jet to market, lower-cost development methods using computer-aided design were also employed in this project.

Under this project, Tohoku University participated as a collaborator and published a number of research results. Obayashi et al. (2005) and Takenaka et al. (2005) provided an overview of the collaborative works. Chiba et al. (2007) and Kumano et al. (2006a) gave an account of the MDO system development for the main wing. Hatanaka et al. (2006) and Kumano et al. (2006b) described the MDO system for engine-airframe integration. The winglet design was performed by Takenaka et al. (2008). Aeroelastic simulations were also performed in the works provided by Kumano et al. (2008) and Morino et al. (2009).

3.1 Definition of optimization problem

The application shown here is the MDO tool for a regional-jet wing design with engine-airframe integration (Kumano et al., 2006b). It should be noted that the optimized wing is not the exact MRJ wing; rather, the acquired design knowledge from the present application has been utilized for the MRJ wing design. Integration is an imperative issue in aircraft design. The shock wave generated inboard of the pylon may lead to flow separation and buffeting. To prevent these phenomena, the wing shape near the pylon has been optimized. The following design objectives are considered here.

<Objective functions>

Minimize

- Drag under cruising conditions (CD).
- Shock strength near wing-pylon junction (–Cp,max).
- Structural weight of the main wing (Wing weight).

<Design variables>

- Airfoil shapes of lower surface at 2 spanwise sections = 26 variables
- Twist angles at 4 sections = 4 variables

30 variables in total

<Constraints>

- Wing thickness > specified value
- Rear spar height > specified value
- Strength margin > specified value
- Flutter margin > specified value

3.2 Optimization results

During the optimization, the update of the Kriging models was performed six times. A total of 149 sample points were used. Figure 4 shows the performance of the baseline configuration and those of additional sample points at every iteration. As the iteration progressed, sample points moved toward the optimum direction indicating that the additional sample points for update were selected successfully. Several solutions with improvements in all objective function values compared with the baseline shape were obtained. One of the solutions was improved in 7.0 counts in C_D, 0.503 in $-C_{p,max}$, and 21.6 kg in the wing weight compared with the performance of the baseline shape.

3.3 Airfoil parameters used in data mining

Data mining was performed using airfoil parameters that differed from non-uniform rational B-spline (NURBS) design variables. The difference is due to the fact that NURBS control points have no aerodynamic or structural significance. Figure 5 shows the airfoil parameters of interest. XmaxL represents the distance from the leading

DOI:10.5139/IJASS.2010.11.4.247

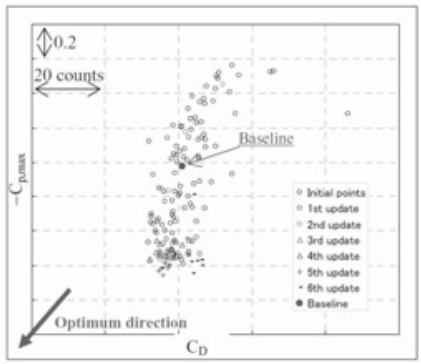

(a) CD - –Cp,max

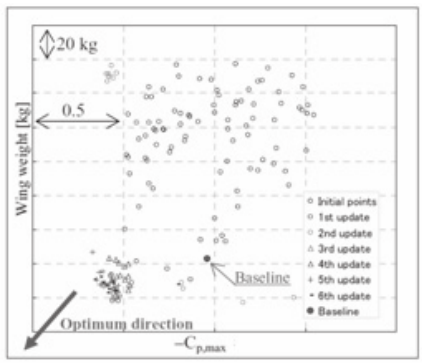

(b) –Cp,max - Wing weight

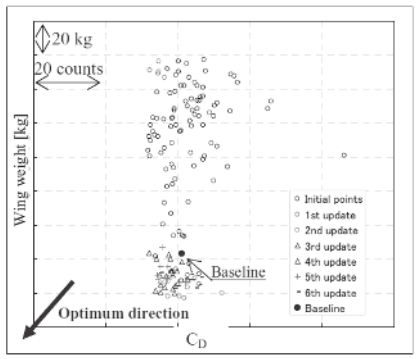

(c) CD - Wing weight

Fig. 4. Comparison of design performance among the baseline shape and sample points through Kriging updates.

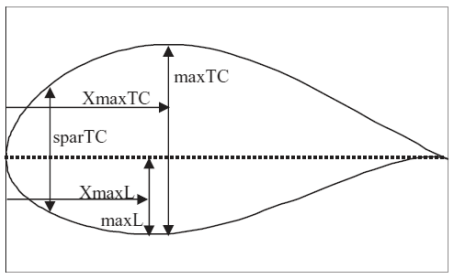

Fig. 5. Airfoil parameters used for data mining.

Table 1. Airfoil parameters used for data mining

Number	Airfoil parameters
dv1	XmaxL @ η = 0.12
dv2	XmaxL @ η = 0.29
dv3	maxL @ η = 0.12
dv4	maxL @ v= 0.29
dv5	XmaxTC @ η = 0.12
dv6	XmaxTC @ η = 0.29
dv7	maxTC @ η = 0.12
dv8	maxTC @ η = 0.29
dv9	sparTC @ η = 0.12
dv10	sparTC @ η = 0.29

edge to the maximum thickness point of the lower half of the airfoil. maxL is the corresponding maximum thickness of the lower half. XmaxTC is the distance from the leading edge to the maximum thickness point. maxTC is the corresponding maximum thickness. In addition, sparTC is the thickness at the front spar. These parameters are taken at two wing sections as shown in Table 1.

3.4 Analysis of variance

ANOVA is a statistical data mining technique that reveals the effects of each design variable on the objective and the constraint functions (Jones et al., 1998). ANOVA uses the variance of the model due to individual variables and pairs of variables (interactions) of the approximation function based on the Kriging model. By decomposing the total variance of the model into components due to main effects and interactions, the influences of individual variables and their pairs on the objective function can be calculated. Because the present Kriging model allows nonlinear approximation, ANOVA is sufficient for the present data mining.

Figure 6 shows the results of ANOVA for each objective function. According to the results, dv2, dv7, and dv9 largely influence CD. dv6, dv10, and dv2 largely influence –Cp,max. Furthermore, dv6, dv8, and dv2 largely influence wing weight.

3.5 Visualization of design space

In order to visualize the design space, SOMs proposed by (Kohonen, 1995) were employed. The following SOMs were generated by Viscovery SOMine (http://www.eudaptics.com/somine. accessed March 5, 2010). Once the user specifies the size of the map, this software automatically initializes the map based on the first two principal axes. The aspect ratio of the map is also determined according to the ratio of the corresponding principal components. The size of the map is usually 2000 neurons, which provides a reasonable

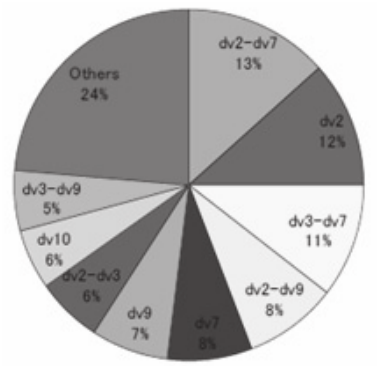

(a) CD

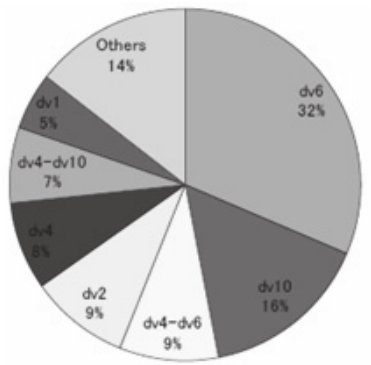

(b) –Cp,max

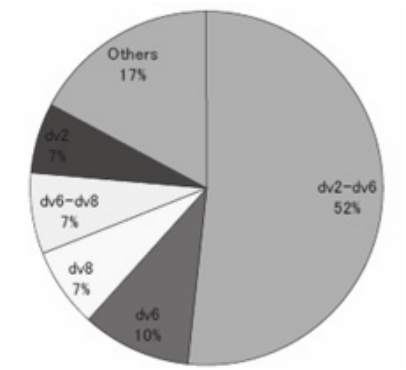

(c) Wing weight

Fig. 6. ANOVA results for each objective function based on airfoil parameters.

resolution within a reasonable computational time.

Solutions uniformly sampled from the design space were projected onto the two-dimensional SOM. Figure 7 shows the resulting SOM with 12 clusters considering the three objectives. Furthermore, Fig. 8 shows the same SOM colored by the three objectives. These color figures show that the SOM indicated in Fig. 7 can be grouped as follows:

- The upper right corner corresponds to the designs

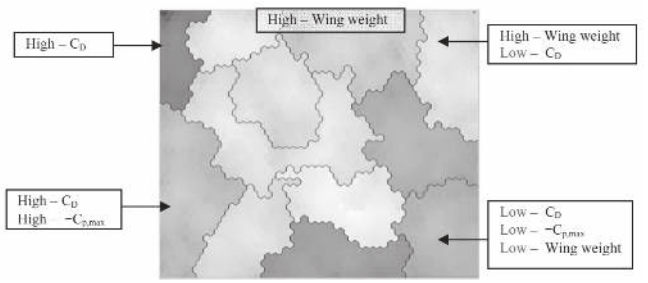

Fig. 7. Self-organizing map based on the design performance uniformly sampled from the design space.

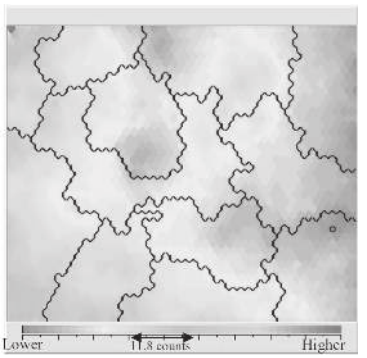

(a) CD

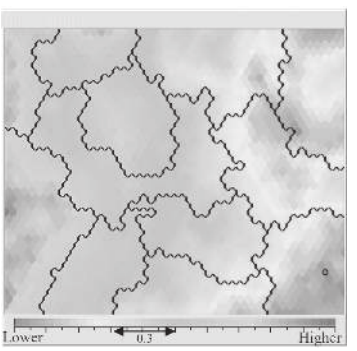

(b) –Cp,max

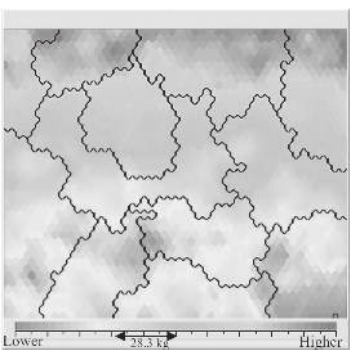

(c) Wing weight

Fig. 8. Self-organizing map based on the design performance colored by each objective function.

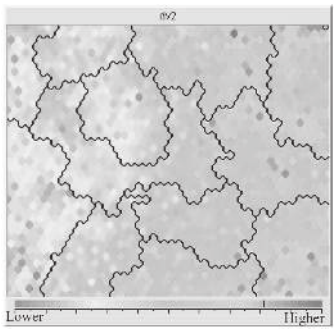

(a) dv2

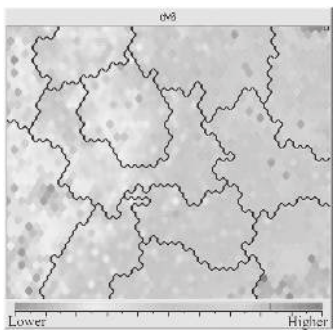

(b) dv6

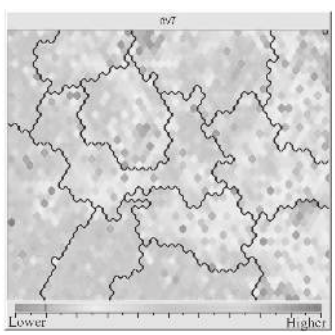

(c) dv7

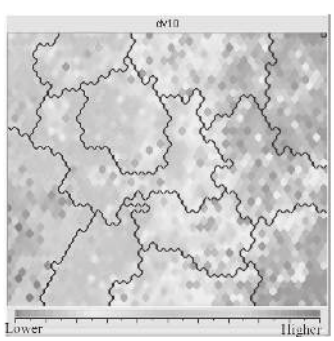

(d) dv10

Fig. 9. Self-organizing map based on the design performance colored by the airfoil parameters.

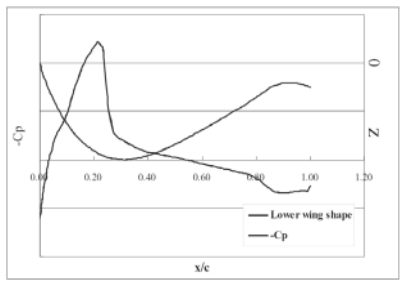

(a) High –Cp,max design

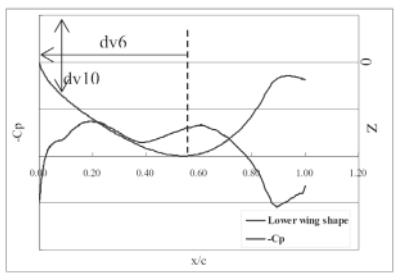

(c) Low –Cp,max design

Fig. 10. Comparisons of airfoil lower surfaces and corresponding pressure distributions near the wing-pylon junction.

containg heavy wing weight and low C_D.

- The upper edge area corresponds to those with heavy wing weight.
- The lower right corner corresponds to those with low C_D, $-C_{p,max}$, and light wing weight.
- The upper left corner corresponds to those with high C_D.
- The lower left corner corresponds to those with high C_D, and $-C_{p,max}$.

As a result, the lower right corner is the sweet spot in this design space, improving all three objective functions.

Figure 9 shows the same SOM colored by four airfoil parameters (dv2, dv6, dv7, and dv10, respectively). In Fig. 9(a) colored by dv2, large dv2 values can be found at the right edge. This area corresponds to small C_D and $-C_{p,max}$ values as shown in Figs. 8(a) and (b), respectively. This signifies that large dv2 values lead to acceptable C_D and $-C_{p,max}$ performance. Furthermore, in Fig. 9(c) colored by dv7, low dv7 values can be found at the right edge. This color pattern is very similar to that for C_D. This also indicates that low dv7 values lead to acceptable C_D performance.

In Fig. 9(b) colored by dv6, large dv6 values can be found at the right edge. This means that large dv6 values lead to good performance of $-C_{p,max}$. In addition, the color pattern of Fig. 9(d) is very similar to that for $-C_{p,max}$. This means that low

dv10 values lead to good performance of $-C_{p,max}$. As shown in Fig. 10, large dv6 and low dv10 values mitigate the blockage between the wing and nacelle. Therefore, the shockwave between the wing and nacelle is weakened.

3.6 Extraction of design rules

Rough set theory was originally developed by Pawlak (1982). This mathematical method has been applied to human sense analysis because of its capability of handling ambiguous data and extracting underlying rules from that data. Because simulation data is deterministic, only the latter function was used. Rough set theory extracts design rules (decision rules) through the classification of set elements and set operations. Since details of the mathematical aspects of rough set theory can be found in the reference, the concept and flowchart of applying rough set theory to an engineering design database are briefly explained using Fig. 11. First, design samples with continuous variables are discretized to make logical set operation possible. Here, design variables are categorized into three levels. Each level is assigned to a different range of values of a design parameter and an objective function in such a way that the levels 1, 2 and 3 correspond to the minimum, middle and maximum ranges, respectively. For objective functions, clusters can be considered as a discrete category instead of these levels. Each design is then regarded as a deterministic rule describing conditions (design variables) and results (objective functions and clusters). Hence, all the data becomes a collection of rule sets. However, the rule sets still have as many conditions as the number of design variables, making it difficult for designers to understand them. Since some design variables do not affect the results or decisions, reducing the number of design variables required to obtain the same results is possible. This operation used for the purpose of obtaining minimum sets of conditions to determine the desired decision attributes is called 'reduct,' which makes obtaining simple rules with fewer conditions possible. Reduct is obtained from set operations. After obtaining reduced rule sets, the rule sets are filtered on the basis of the frequency to determine dominant rule sets. Finally, the meaning of the filtered rule sets is interpreted. Open software ROSSETA (Ohrn, 2000) was used for the necessary calculations.

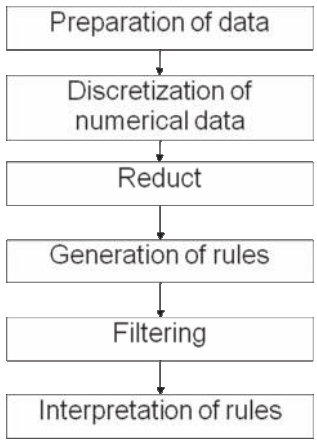

Fig. 11. Flowchart of data mining using rough set theory.

Table 2. Frequency of appearance in design rules (+ indicates large, - indicates small and no sign indicates medium)

	Sweet	Cd	-Cp	WW
dv1	11	1	+1	5
dv2	+9	+2	+6	+3
dv3	8	-5	6	4
dv4	+10	-3	+5	+11
dv5	13	+8	+1	7
dv6	+7	+6	+3	+3
dv7	9	-5	-6	5
dv8	2	-4	3	2
dv9	-9	-2	-2	-3
dv10	-14	-9	-8	-8

The resulting rule appears, for example, 'dv1(medium) AND dv2(large) AND dv5(medium) AND dv7(medium) AND dv9(small) AND dv10(small) => Cluster(C6), occurrence(10).' It still appears complicated because the condition consists of a combination of five design parameters. In order to interpret the design rules more comprehensively, the frequency of appearance of small, medium and large for each design parameter was counted according to the sweet-spot cluster, small objective function values (CD, $-C_{p,max}$ and wing weight), respectively, as summarized in Table 2. For example, dv2-sweet reads +9. This signifies that the condition dv2(large) appears 9 times among the rules to belong to the sweet spot cluster. In other words, to belong to the sweet spot cluster, dv2, dv4 and dv6 should be large and dv9 and dv10 should be small.

The design knowledge discussed by using SOM in Section 3.3 can be summarized as

1) Large dv2 improves C_D and $-C_p$.

2) Small dv7 improves C_D.

3) Large dv6 improves $-C_p$.

4) Small dv10 improves $-C_p$.

Table 2 exhibits information consistent with these visualization results. Table 2, however, provides much more than the visualization. For example, dv4 should be large in order to belong to the sweet spot cluster, but it should be small in order to improve only the drag. Similarly, dv7 should be medium although it should be small in order to improve C_D and $-C_p$. This illustrates the power of rough set theory.

Visualization results depend on who looks at the figures and how deeply one reads. The result of rough set theory reduces oversights and reveals more detailed conditions.

4. Two-Step MDO for S3TD Airplane

Since the flight experiment of the non-powered supersonic experimental scaled airplane NEXST-1 succeeded in October 2005 (Ohnuki et al., 2006), research and development of the S3TD has garnered the focus of the Japan Aerospace Exploration Agency (JAXA) (Murakami, 2006).

This paper presents the practical two-step multidisciplinary design exploration (MDE) for S3TD airplane. The wing planform was re-designed in order to improve lift performance at low speeds and also to restrain low boom performance for wing-fuselage simple configuration. Then, a three-dimensional main wing and a stabilizer were designed for intimate configuration constructed as the main wing, fuselage, vertical tail wing, stabilizer, and engine system.

4.1 design-exploration system

4.1.1 Optimizer

A hybrid method between particle swarm optimization and genetic algorithm was employed. Recent optimization work often used a response surface model (RSM) based on a Kriging surrogate model in order to restrain evaluation time (Jeong et al., 2005b). However, when the optimization problem with many design variables is taken into consideration, many initial sample points are needed to maintain the accuracy of the response surface. In the present study, RSM was not selected in order to avoid extensive evaluation time for the initial samples. In addition, since the designers were required to present many optimum solutions for the decision of a compromised one, an evolutionary-based Pareto approach as an efficient multi-thread algorithm was employed instead of a gradient-based method.

4.1.2 Data mining

Although design optimization is important for engineering, the most significant design consideration is the extraction of knowledge in a design space. The results obtained by multiobjective (MO) optimization are not a sole solution, but an optimum set. That is, MO optimization results are insufficient information for practical design because designers need a conclusive shape. However, the results acquired from MO optimization can be accounted for as a hypothetical design database. Data mining as a post-process for optimization is essential for efficiently obtaining fruitful design knowledge (Obayashi and Sasaki, 2003). In the present study, functional ANOVA (Sobol, 1993) and a SOM (Deb, 2001) were used for data mining. The distinguishing feature of a SOM is the generation of a qualitative description. When two methods are combined together, the results obtained compensate for the disadvantages of the individual methods (Chiba and Obayashi, 2008).

4.1.3 Evaluation methods

The present exploration system prepared three evaluation modules for aerodynamics (including stability), structures, and boom noise. It took roughly seven days to evaluate one generation using the central numerical simulation system (CeNSS) of Numerical Simulator III in JAXA.

1) Aerodynamic evaluation: TAS-Code, parallelized unstructured Euler/Navier-Stokes solver was employed. Three-dimensional Euler equations were solved with a finite-volume cell-vertex scheme on the unstructured mesh (Ito and Nakahashi, 2002).

2) Structural evaluation: In the present MDE systems, structural optimization was performed in order to realize minimum wing weight with constraints of strength, vibration, and flutter requirements. The strength, vibration, and flutter characteristics were evaluated by using the commercial software MSC. NASTRANTM.

3) Sonic boom evaluation: The computer-aided design-based automatic panel analysis system (CAPAS) (Makino and Naka, 2007) was used.

4.2 First-step multidisciplinary design exploration

MDE was defined in the consideration of the sequence of the projecting flight experiment. The initial 0th shape of S3TD was designed to focus on low boom and low drag. However, its shape exhibited insufficient performance in regards to lift at low speed. Therefore, the second shape with a primary purpose of lift-performance improvement would be re-designed to maintain low boom intensity (the first shape was for minor change to re-design low-boom geometry). Detailed information of this MDE work is provided in Chiba et al. (2008).

4.2.1 Objective functions

The following five objective functions were defined. The first three objective functions are for aerodynamics, the fourth is for noise, and last is for structures.

1) The minimization of the pressure drag at supersonic cruising condition: $S \bullet C_{Dp}$ (Mach number of 1.6, altitude of 16 km, and target C_L of 0.132 for the reference configuration of S^{3}TD. $S \bullet C_L^{\text{supersonic}} = \text{const}$. S denotes the one-sided wing reference area).

2) The minimization of the friction drag at supersonic condition: $S \bullet C_{Df}$. In this study, since the Prandtle-Hoerner's simple equation was used for C_{Df} evaluation, the each fidelity of C_{Dp} and C_{Df} was different. Therefore, the objective functions were separated to avoid disappearing one influence for the inconsistency.

3) The maximization of the lift at subsonic condition: $S \bullet C_L$ (Mach number of 0.2 and angle of attack of 10.0 deg).

4) The minimization of sonic boom intensity I_{boom} at supersonic condition. This objective function value was defined as $|\Delta P_{max}| + |\Delta P_{min}|$ at the location with largest peak of sonic-boom signature across boom carpet.

5) The minimization of a composite structural weight W_c for wing using fiber angle of ply and a number of ply with the fulfillment of the strength and vibration requirements. When an individual could not be satisfied with the requirements, the penalty was given to the rank in the optimizer.

The present objective functions were selected in order to define no constraint conditions due to tradeoffs. Tradeoffs were expected between $S \bullet C_{Dp}$ and Wc as well as that between $S \bullet C_{Dp}$ and $S \bullet C_L$.

4.2.2 Decision of a compromise solution from design-exploration results

The total evolutionary computation of 12 generations was performed, and 75 non-dominated solutions were obtained. Here, the derived non-dominated solutions are focused because a compromise solution was selected. The evolution might not converge yet. However, the result was satisfactory because several non-dominated solutions achieved improvements over the reference configuration. Furthermore, a sufficient number of solutions were searched so that data mining of the design space can be performed. This provides useful knowledge for designers.

The 75 non-dominated solutions were extracted using an SOM in order to determine a compromise solution. The applicable solutions to the following conditions were excluded from the 75 non-dominated solutions: 1) The structural requirements were not fulfilled, 2) $S \bullet C_L$ is low, or wing area was low (this means the constraint for the landing speed), 3) $S \bullet C_{Dp}$ and $S \bullet C_{Df}$ were impractically large. As a result of this operation, 24 non-dominated solutions as the practical designs were sorted. The SOM was re-generated using derived 24 non-dominated solutions taking into consideration the five objective functions. The compromise solution was determined from these individuals taking into consideration the balance of the five objective functions and the low-boom competence as the primary objective of the S^{3}TD on SOM. The designers clustered similar planform shapes, and selected the exploitable shape group as a demonstrator using

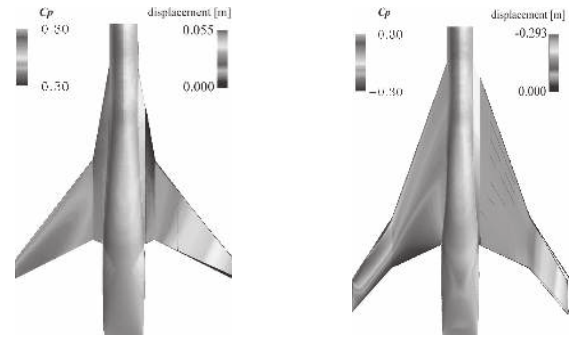

(a) Reference configuration (b) Compromise solution

Fig. 12. Comparison of wing shape colored by Cp and displacement distributions.

the experiences cultivated by the development of real-world aircrafts. Four shapes were selected taking into consideration the low-boom competence. The final compromise solution which is improvable due to the refinements on the fuselage and cross-section geometries was ultimately determined.

Since the compromise solution secured the wing area, low-speed aerodynamic performance could be improved and it was re-designed to have practical capability for takeoff and landing. However, as the objective functions regarding aerodynamics depended on wing area, the design knowledge about wing cross section was insufficient.

A comparison of the planform between the reference configuration and the selected compromise solution (called '*compromise*') is shown in Fig. 12. Also, airfoils of the reference and *compromise* configurations near the junction relative to the fuselage, kink, and tip are shown. It is notable that the reference configuration does not possess twists, and its airfoil is described by NACA64A series. The thickness ratios are respectively defined as 6% at root, 5% at kink, and 3% at tip. The installed angle of the wing is –0.5 deg relative to the fuselage. As $S \bullet C_L$ is the maximization objective, *compromise* has a larger wing area than that of the reference configuration. Furthermore, the inner wing area of *compromise* becomes large as a means of securing the structural strength. The sweepback angle was more subtle so as to not affect I_{boom}. Thus, the wing area and structural strength are also secured. But, the chord length near the kink was designed short in order to achieve low W_c and $S \bullet C_{Df}$. Therefore, the number of ply increased to augment the eigen frequency. The supersonic leading edge of compromise was located near the root in order to reduce the effect on I_{boom} of the front boom. Also, the blunt leading edge of *compromise* was located near the kink in order to improve the strength, eigen frequency, and subsonic aerodynamic performance. Data-mining results indicate that the sharp leading edge

near the tip affects I_{boom}. But, the wing area provides a strong effect on the objectives. Therefore, the knowledge regarding the airfoil shape is unreliable.

Finally, the boom intensity as the primary objective function was *compared* between the reference and compromise configurations. Although I_{boom} performance of the reference configuration was better, *compromise* also maintained a non-N-shaped signature to restrain the initial peak. *Compromise* exhibited better $S \bullet C_L$ performance for the landing speed constraint as well as the I_{boom} restraint. In this study, the rearward boom intensity cannot be discussed because the assumed fuselage-wing configuration ignores an engine nacelle and vertical/horizontal tail wings. But, computational fluid dynamics (CFD) visualization of C_p distribution on symmetrical plane reveals that shock wave occurs in the vicinity of wing trailing edge. It is necessary that the full configuration is optimized to design the geometry restrained rearward boom intensity and to obtain the design knowledge regarding cross section shape.

4.3 Second-step multidisciplinary design exploration

Second-step MDE was implemented among aerodynamics, stability, structures, aeroelasticity, and boom noise. An intimate configuration of the 2.5th latest shape composed by main wing, fuselage, vertical tail wing, stabilizer, and engine system was considered in order to strictly evaluate each objective. As the 2.5th shape did not trim, the geometry design to trim is the primary objective of this optimization. The optimization target was the airfoil shapes of the main wing cross section at root, kink, and tip positions, and the deflection angle of the stabilizer. This MDE work is explained in detail in Chiba et al. (2009).

4.3.1 Objective functions

1) The minimization of the pressure drag C_{Dp} at supersonic cruising, which is defined by a Mach number of 1.6, altitude of 14 km, and target C_L of 0.055. The target C_L is constant due to the fixed planform.
2) The minimization of the intensity of sonic boom I_{boom} at supersonic cruising. This objective function value is defined as $|\Delta P_{max}| + |\Delta P_{min}|$ at the location with the largest (smallest) peak of sonic-boom signature across boom carpet.
3) The minimization of structural weight W for a main wing. The inboard and outboard wings are respectively defined as aluminum and composite materials. The minimum wing weight is solved with the fulfillment of the strength and flutter requirements. For the inboard wing made of aluminum, the thicknesses of skin and multi-frames are optimized. In addition, for the outboard wing made of composite material, the stacking sequence is optimized. These are the combination optimizations, and these are the nesting constitution for the present MDO.
4) The minimization of the difference between the centers of pressure and of gravity $|x_{cp} - x_{cg}|$ to trim. "MAC" denotes mean aerodynamic chord. The center of pressure is calculated as follows.

$$x_{cp} = x_{ref} - \frac{C_{Mp}}{\text{target}C_L} \times \text{MAC}$$
$$x_{ref} = 25\%\text{MAC} \tag{1}$$

On the other hand, the center of gravity x_{cg} is computed from the aerodynamic center N_0 as follows.

xcg = N0 – const.

$$x_{cg} = N_0 - \text{const.} = x_{ref} - \frac{\Delta C_{Mp}}{\Delta C_L} \times \text{MAC} - \text{const.} \tag{2}$$

where, the constant value const. in Eq. (2) is defined by the results of Navier-Stokes computations in advance. It is set on 0.817 m in this study.

4.3.2 Selection and evaluation of compromise solution from design-exploration results

The total evolutionary computation of 18 generations was performed using 139 individuals, and 37 non-dominated solutions were obtained. The concrete presented materials roughly classify into two groups.

One group comprises information regarding tradeoffs among the objective functions. The other group is composed of information concerning the candidates of a compromise solution. This includes the contour figure of the C_p distribution at a supersonic cruising condition (shown in Fig. 13), the wing section and C_p distribution at root (21.62% spanwise location), kink (63.33%), and tip (99.00%). Moreover, the candidates are selected from the non-dominated solutions and individuals adjacent to them, which indicate the relationship between the boom intensity and the trim performance. The boom intensity has priority in this study. The trim performance provides tradeoffs for all of the other objective functions. The individual with complicated manufacturing is excluded as a candidate of the compromise solution. The important points are: 1) the performance of all objective functions, and 2) the possibility for the improvement of the other three objectives to maintain boom performance. On the final decision for

(a) Upper surface view

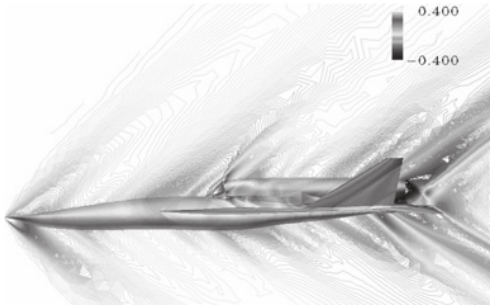

(b) Symmetrical-plane view

Fig. 13. C_p distribution of the decided compromise solution. The angle of attack of 2.915deg is set to achieve the target C_L.

Table 3. The specification of the selected compromise solution

C_{Dp}	0.02092
I_{boom}	0.9301 psf
W	341.3 kg
$\|x_{cp}-x_{cg}\|$	1.065 m
Outboard wing	8 plies * 4 sets
Inboard wing	skin: 9.0 mm, multi frames: 8.9 mm
Design angle of attack	2.915 deg
Reflection angle of stabilizer	-1.608 deg

a compromise solution, the individual with a wing section similar to NEXST-1 was selected. That is, the shape of the selected compromise solution is more feasible regarding aerodynamics and manufacture. The conclusion followed that trim performance was improved by the regulation of the reflection angle of the stabilizer (the outside range set in the present optimization is namely reconsidered). Therefore, a weak non-dominated solution was selected as a compromise solution.

Table 3 shows the specification of the compromise solution. It is notable that the criteria of the design angle of attack and the reflection angle of the stabilizer is the horizontal line (longitudinal axis of body) for three views. Thus, the reflection angle is defined for the longitudinal axis of the body and is independent of the angle of attack. This result shows that the trim performance is insufficient. The results from ANOVA indicate that the cant angle and the geometry of the main wing, which influence trim performance, affect several objective functions. However, the reflection angle of the stabilizer does not affect any objective function with the exception of the trim performance. Since the designed reflection angle of the stabilizer can afford to be harder, its modification can improve the trim performance.

Figure 13 shows the C_p distributions on the upper surface and on the symmetrical plane. This figure reveals that the shock waves occur around the front location of the engine and bumps into the upper surface of the main wing. Although the shock wave is shielded, the performance of the wing is degraded. It is important to design the geometry of the wing for the alleviation of this shock wave. At the root location, since two shock waves bump into the wing upper surface, the increase of the wing thickness provides insufficient lift performance and augments the induced drag. On the other hand, it reveals the connection between the structural weight and the structural requirements. The constraint of the thickness at the root is 5% ± 1% chord length. The thickness of the compromise solution at the root is 4.4% chord length. Its thickness becomes thin with the fulfillment of the structural requirements. The upper surface near the leading edge at the kink location is dented. Therefore, the shock wave occurred from the front of the engine is mitigated. The pressure distribution also indicates the similar effect. This hollow component is the key necessary for improving the aerodynamic performance. The maximum thickness at the kink is 5.4% chord length. The thickness at the kink location should be thick in order to provide sufficient aerodynamic performance and to fulfill the structural requirements. At the tip location, the wing exhibits insufficient aerodynamic performance. Since the wing geometry in the vicinity of the tip strictly affects the boom intensity indicated by the data-mining results, the wing tip geometry is evolved to reduce the boom intensity. In addition, a strong shock wave occurs around the rear part of the fuselage. As this corrupts the rear boom intensity, re-consideration is needed.

The ground pressure signature of the compromise solution indicates that both peaks of the front and rear boom intensity are weakened because it is not N shape. The data mining reveals that three design variables for the main wing such as the cant angle for the attachment to the fuselage, twisting angle, and the bluntness of the leading edge affects the front boom. It similarly reveals that the design variable as the reflection angle of the stabilizer affects the rear boom. In particular, the inboard wing with a camber on the trailing edge improves the rear boom intensity. The strong expansion wave from the trailing edge extinguishes the positive pressure from the lifting surface of the rear fuselage. Moreover, the large negative reflection angle of the stabilizer causes strong rear boom intensity due to a similar reason. However, the negative reflection angle must be trimmed. The reflection angle of the stabilizer is essential in the present

design problem.

The two multidisciplinary design explorations for the silent supersonic technology demonstrator were demonstrated. The process of this approach provided tradeoffs among the defined design requirements, i.e., objective functions. Furthermore, the important design variables were evident, and the correlations between the design requirements and the variables were also shown. The obtained design information was produced for the designers, and it was employed as the resource of decision making in order to determine a compromise solution. The knowledge was produced for future design.

5. Performance Studies for Centrifugal Diffusers

This study discusses further applicability of data mining techniques (ANOVA and SOM) to a fundamental topic in engineering research, i.e., the construction of performance maps that represent relations between performance and geometry parameters. Performance maps are often used to make a first decision on preliminary specification of a product to be designed. Therefore, performance map construction is an essential area in the field of engineering.

This study was performed using a *centrifugal diffuser* as the target product for performance map construction. The centrifugal diffuser is one a component commonly used in various household appliances (air cleaners, vacuum cleaners, etc.) as well as heavy industrial machineries (aircraft engines, marine engines, etc.). Conventionally, diffuser performance has been evaluated based on the quasi-one-dimensional nozzle theory. Figure 14 illustrates the performance map for a linear nozzle with a rectangular cross-section, which

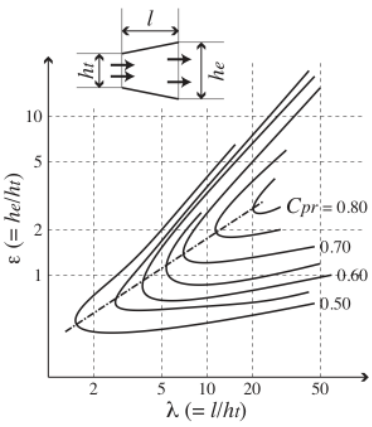

Fig. 14. Performance map for a linear nozzle with rectangular cross-section (Ikui, 1988).

mimics the original map in Ikui (1988). This map represents the contour lines of the pressure recovery coefficient C_{pr} in the nozzle throat to exit section, which are plotted on the plane taking two nozzle geometry parameters into consideration (aspect ratio λ and expansion ratio ε). It reveals the C_{pr} vs. λ and C_{pr} vs. ε relationships, which are suitable for diffusers with flat blades. However, actual diffusers mostly consist of cambered blades, and actual diffuser performance seems to be affected by the blade geometries ignored in the quasi-one-dimensional nozzle theory (blade camber, blade attack angle to flow, etc.). In addition, diffuser hub and case geometries may also affect diffuser performance (*e.g.*, Kitadume et al. (2007) discuss the case geometry effects based on experiments). A further consideration is that actual diffusers should ensure good overall performance, i.e., air pressure must be recovered not only in the nozzle section but also upstream and downstream of the nozzle. Thus, the performance map should be constructed in a higher-dimensional form, which allows comprehension of the various relationships among many performance parameters and many geometry parameters. Therefore, the centrifugal diffuser is an appropriate target product to validate the data mining techniques for high-dimensional performance map construction, as well as to provide useful knowledge about the relations between diffuser performance and geometries.

The performance studies for centrifugal diffusers have also been reported by other researchers. Krain (1981) experimentally measured the internal flow field development within an impeller-diffuser-interacted stage by means of laser velocimeters. Simon et al. (1987) experimentally investigated simultaneous adjustments of inlet guide blades and diffuser blades in centrifugal compressors for the improvements in both performance and operating range. Paxson and Skoch (1998) proposed and demonstrated a wave augmented diffuser that reduces the loss caused by the discharge flow turning from a radial or tangential direction to an axial direction by numerical simulations. However, diffuser geometries considered in those studies were limited to flat blades (Krain, 1981; Paxson and Skoch, 1998) or cambered blades parameterized simply by the angle of attack (Simon et al.,1987). Although Kim et al. (2009) compared and discussed the performance among three different diffusers (wedge, symmetric airfoil, and cambered airfoil) by numerical simulations, it still was lacking in the varieties of diffuser geometries that could be considered for performance map construction. In a recent study conducted by Abdelwahab and Gerber (2008), a three-dimensional aerofoil diffuser geometry, which allows spanwise variations in solidity, stagger, and lean angles, was developed for industrial centrifugal compressor stages based on both

numerical and experimental analyses. But its performance tendencies have not been explained in a high-dimensional form of geometry parameters.

5.1 Geometry and performance definition of centrifugal diffusers

Figure 15 shows the centrifugal diffuser geometries considered in this study. This diffuser has 13 similar cambered blades of constant thickness. The leadi ng and trailing edges of these blades are linear and parallel to the diffuser center axis. The diffuser geometries are defined by the blade size (D_3 and D_4 shown in Fig. 15(a)), the case size (D_5 and D_{ex} shown in Fig. 15(a)), and the blade camber angle (β_3 and β_4 shown in Fig. 15(b), where a linear profile is assumed between the leading and trailing edges). For simplicity, this study fixed D_3 and generated 100 diffusers with different shapes through the Latin hypercube sampling (LHS) (McKay et al., 1979), in which the values of D_4/D_3, D_5/D_4, D_{ex}/D_5, β_3, and β_4 were treated as five independent random variables for geometry definition of the diffuser. As described in the next section, this study implemented the data mining for performance map construction based on 12 geometry parameters in the nozzle part (h_t, h_e, l_p, l_s, l_{avg}, θ, α, κ_p, κ_s, κ_{avg}, ε, and λ shown in Fig. 15(c)) instead of the five random variables considered in LHS.

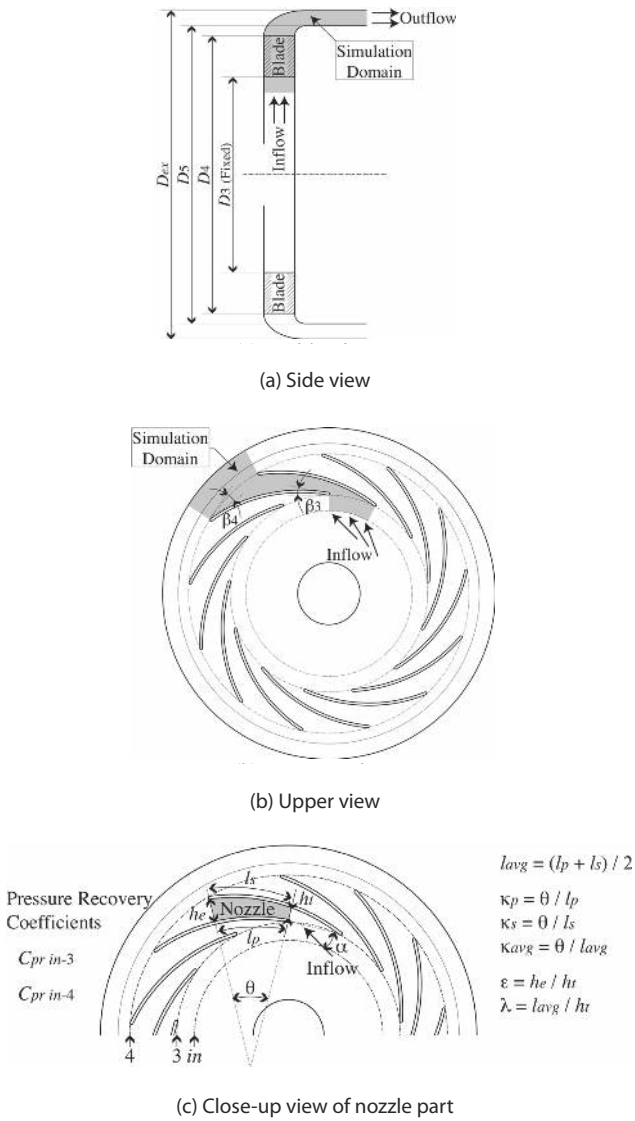

Fig. 15. Centrifugal diffuser geometries.

The centrifugal diffuser should work so efficiently that it can to decelerate internal air flow without pressure loss. In general, such performance can be quantified by a pressure recovery coefficient such that a larger value of the coefficient leads to more efficient air deceleration. For general discussions on diffuser performance, this study focused on two pressure recovery coefficients in different sections as performance functions: $C_{pr\ in\text{-}3}$ for inlet to blade entrance section and $C_{pr\ in\text{-}4}$ for inlet to blade exit section. This study was performed to evaluate the values of $C_{pr\ in\text{-}3}$ and $C_{pr\ in\text{-}4}$, which were obtained at a constant mass flow rate, from the CFD simulations for 100 different diffusers generated by LHS. The present CFD simulations solved the Reynolds-averaged Navier-Stokes (RANS) equations for compressible air, which were coupled with the high-Reynolds-number k-ε turbulence model, using the commercial software STAR-CD™ (http://www.cd-adapco.com. accessed April 1, 2009). Consequently, in the present implementation, the performance values were successfully obtained for 85 diffusers, while the CFD simulations fell into divergence for the rest.

5.2 Data mining results and discussion

Figure 16 shows the data mining results obtained by ANOVA. Figures 16(a) and (b) show the breakdowns of the main effects and the interaction effects for each performance function. For $C_{pr\ in\text{-}3}$, only the variable h_t (throat width) has a major contribution. For $C_{pr\ in\text{-}4}$, although various contributions of h_t, κ_p (pressure side curvature), ε (expansion ratio), and λ (aspect ratio) were revealed, a combination of two variables, h_t and κ_p, has the largest contribution. Figures 16(c) and (d) shows the functional-formed main and interaction effects of the variables that showed large contributions in Figs. 16(a) and (b), respectively. Figure 16(c) indicates that smaller h_t leads to larger $C_{pr\ in\text{-}3}$. Figure 16(d) indicates that a combination of smaller h_t and larger κ_p, and a combination of larger h_t and smaller κ_p lead to larger $C_{pr\ in\text{-}4}$.

Figures 17 shows the SOM color images, each of which is colored according to performance or nozzle geometry parameters (only four nozzle geometries with large

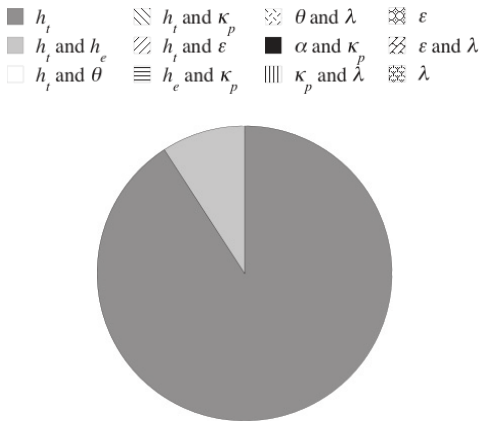

(a) Breakdowns of main and interaction effects on $C_{pr\,in\text{-}3}$

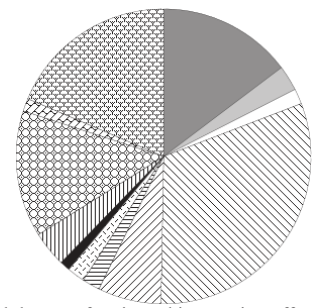

(b) Breakdowns of main and interaction effects on $C_{pr\,in\text{-}4}$

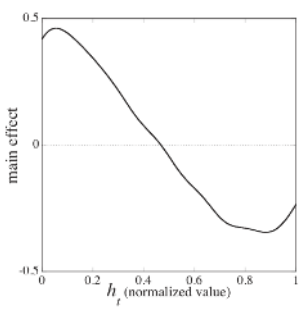

(c) Functional main effect of h_t on $C_{pr\,in\text{-}3}$

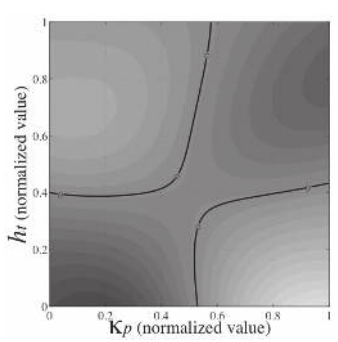

(d) Functional interaction effect of h_t vs. κ_p on $C_{pr\,in\text{-}4}$

Fig. 16. ANOVA data mining results.

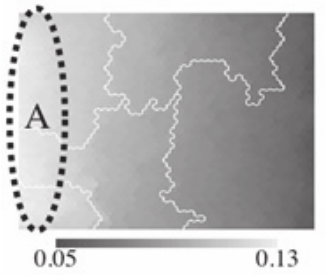

(a) $C_{pr\,in\text{-}3}$

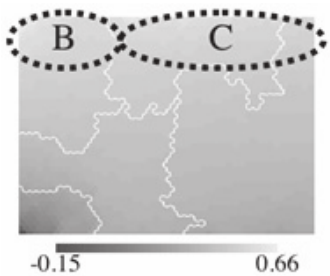

(b) $C_{pr\,in\text{-}4}$

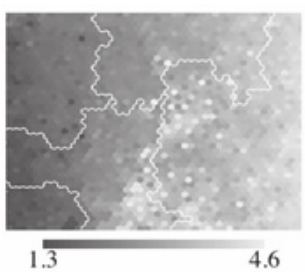

(c) h_t

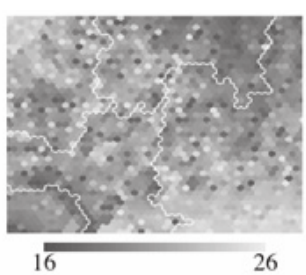

(d) κ_p

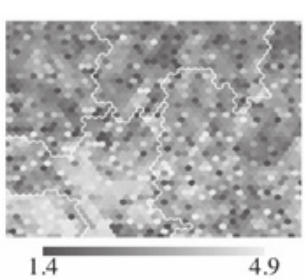

(e) ε

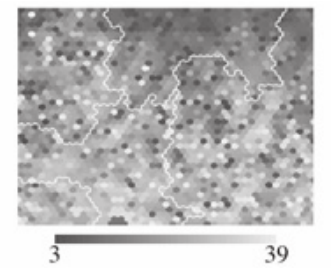

(f) λ

Fig. 17. Self-organizing map data mining results.

contributions are considered here). $C_{pr\ in\text{-}3}$ becomes large in the left area on the SOM (denoted as "A" in Fig. 17(a)), while h_t becomes small in this area. This relation is consistent with the main effect results given by the ANOVA, as shown in Fig. 16(c). Conversely, $C_{pr\ in\text{-}4}$ becomes large in the upper area on the SOM, which is denoted as a combination of "B" and "C" in Fig. 17(b). Area B has small h_t and large κ_p, while area C has large h_t and small κ_p. Therefore, each of areas B and C is also consistent with the interaction effect results from the ANOVA in Fig. 16(d). Furthermore, other higher-order interaction effects can also be determined by comparing the color patterns of all the SOM images. Thus, the SOM color images can serve as the high-dimensional performance maps themselves.

Among the results obtained in the present data mining, the interaction effect of h_t and κ_p is a remarkable issue to discuss diffuser performance because κ_p is not considered in the quasi-one-dimensional nozzle theory (Fig. 14). The present results specify a large effect of the blade curvature on the pressure recovery performance in the diffuser with a curved nozzle. Therefore, this study confirmed that data mining techniques can be used to discover new engineering knowledge, and is suitable and applicable to performance map construction with high dimensions.

6. Conclusions

This article reviewed existing visual data mining techniques that had been formally applied to engineering problems. We discussed three applications of MODE: MDO for the regional-jet wing, the S3TD and centrifugal diffusers. With the given set of design parameters, ANOVA was first applied. The results indicated which design parameters were influential. Next, visual data mining for the design space was performed using SOM. SOM divided the design space into clusters with specific design features. SOM obtained from the solutions uniformly sampled from the design space revealed that the sweet spot could exist. By comparing the SOM colored by influential design parameters found by ANOVA and the objective functions, several design rules were extracted. Finally, sufficient conditions belonging to the sweet spot cluster were extracted by rough set theory. Similarly sufficient conditions to improve each design objectives were extracted. The use of data mining will provide more knowledge about the design space and extract more information from the optimization process.

References

Abdelwahab, A. and Gerber, G. (2008). A new three-dimensional aerofoil diffuser for centrifugal compressors. *Proceedings of the Institution of Mechanical Engineers, Part A: Journal of Power and Energy*, 222, 819-830.

Agrawal, G., Lewis, K., Chugh, K., Huang, C. H., Parashar, S., and Bloebaum, C. L. (2004). Intuitive visualization of Pareto Frontier for multi-objective optimization in n-dimensional performance space. *10th AIAA/ISSMO Multidisciplinary Analysis and Optimization Conference*, Albany, NY. pp. 1523-1533.

Agrawal, G., Parashar, S., and Bloebaum, C. L. (2006). Intuitive visualization of hyperspace pareto frontier for robustness in multi-attribute decision-making. *11th AIAA/ISSMO Multidisciplinary Analysis and Optimization Conference*, Portsmouth, VA. pp. 729-742.

Alpern, B. and Carter, L. (1991). The Hypebox. *IEEE Visualization Conference*, San Jose, CA. pp. 133-139.

Chernoff, H. (1973). The use of faces to represent points in K-dimensional space graphically. *Journal of the American Statistical Association*, 68, 361-368.

Chiba, K., Makino, Y., and Takatoya, T. (2008). Evolutionary-based multidisciplinary design exploration for the silent supersonic technology demonstrator wing. *Journal of Aircraft*, 45, 1481-1494.

Chiba, K., Makino, Y., and Takatoya, T. (2009). Design-informatics approach for intimate configuration of silent supersonic technology demonstrator. *47th AIAA Aerospace Sciences Meeting including the New Horizons Forum and Aerospace Exposition*, Orlando, FL. pp. AIAA 2009-0968.

Chiba, K. and Obayashi, S. (2008). Knowledge discovery for flyback-booster aerodynamic wing design using data mining. *Journal of Spacecraft and Rockets*, 45, 975-987.

Chiba, K., Oyama, A., Obayashi, S., Nakahashi, K., and Morino, H. (2007). Multidisciplinary design optimization and data mining for transonic regional-jet wing. *Journal of*

Aircraft, 44, 1100-1112.

Cios, K. J., Pedrycz, W., and Swiniarski, R. (1998). *Data Mining Methods for Knowledge Discovery*. Boston: Kluwer Academic Publishers.

Deb, K. (2001). *Multi-Objective Optimization Using Evolutionary Algorithms*. New York: John Wiley & Sons.

Eddy, J. and Lewis, K. E. (2002). Visualization of multidisciplinary design and optimization data using cloud visualization. *Proceedings of Design Engineering Technical Conferences*, Montreal, Quebec. pp. 899-908.

Graening, L., Menzel, S., Hasenjager, M., Bihrer, T., Olhofer, M., and Sendhoff, B. (2008). Knowledge extraction from aerodynamic design data and its application to 3D turbine blade geometries. *Journal of Mathematical Modelling and Algorithms*, 7, 329-350.

Hatanaka, K., Obayashi, S., and Jeong, S. (2006). Application of the variable-fidelity MDO tools to a jet aircraft design. *25th International Congress of the Aeronautical Sciences*, Hamburg, Germany.

Holden, C. M. E. and Keane, A. J. (2004). Visualization methodologies in aircraft design. *10th AIAA/ISSMO Multidisciplinary Analysis and Optimization Conference*, Albany, NY. pp. 1685-1697.

Ikui, T. (1988). *Turbo-Blowers and Compressors*. Tokyo, Japan: Corona Publishing Co., Ltd. (in Japanese).

Inselberg, A. (1997). Parallel coordinates for visualizing multidimensional geometry. In Statistical Office of the European Communities, ed. *New Techniques and Technologies for Statistics II: Proceedings of the Second Bonn Seminar*. Washington, DC: IOS Press. pp. 279-288.

Inselberg, A. and Dimsdale, B. (1990). Parallel coordinates: A tool for visualizing multi-dimensional geometry. *Proceedings of the First 1990 IEEE Conference on Visualization*, San Francisco, CA. pp. 361-378.

Ito, Y. and Nakahashi, K. (2002). Direct surface triangulation using stereolithography data. *AIAA Journal*, 40, 490-496.

Jeong, M. J., Kobayashi, T., and Yoshimura, S. (2007). Multidimensional visualization and clustering for multiobjective optimization of artificial satellite heat pipe design. *Journal of Mechanical Science and Technology*, 21, 1964-1972.

Jeong, S., Chiba, K., and Obayashi, S. (2005a). Data mining for aerodynamic design space. *Journal of Aerospace Computing, Information and Communication*, 2, 452-469.

Jeong, S., Murayama, M., and Yamamoto, K. (2005b). Efficient optimization design method using kriging model. *Journal of Aircraft*, 42, 413-420.

Jeong, S. and Obayashi, S. (2005). Efficient Global Optimization (EGO) for multi-objective problem and data mining. *IEEE Congress on Evolutionary Computation*, Edinburgh, Scotland. pp. 2138-2145.

Jones, D. R., Schonlau, M., and Welch, W. J. (1998). Efficient Global Optimization of Expensive Black-Box Functions. *Journal of Global Optimization*, 13, 455-492.

Keane, A. J. (2003). Wing optimization using design of experiment, response surface, and data fusion methods. *Journal of Aircraft*, 40, 741-750.

Kim, H. W., Park, J. I., Ryu, S. H., Choi, S. W., and Ghal, S. H. (2009). The performance evaluation with diffuser geometry variations of the centrifugal compressor in a marine engine (70 MW) turbocharger. *Journal of Engineering for Gas Turbines and Power*, 131, 012201-1-7.

Kitadume, M., Kawahashi, M., Hirahara, H., Uchida, T., and Yanagawa, H. (2007). Experimental analysis of 3D flow in scroll casing of multi-blade fan for air-conditioner. *Journal of Fluid Science and Technology*, 2, 302-310.

Kodiyalam, S., Yang, R. J., and Gu, L. (2004). High-performance computing and surrogate modeling for rapid visualization with multidisciplinary optimization. *AIAA Journal*, 42, 2347-2354.

Kohonen, T. (1995). *Self-Organizing Maps*. Berlin: Springer.

Krain, H. (1981). A study on centrifugal impeller and diffuser flow. *Journal of Engineering for Power, Transactions of the ASME*, 103, 688-697.

Kumano, T., Jeong, S., Obayashi, S., Ito, Y., Hatanaka, K., and Morino, H. (2006a). Multidisciplinary design optimization of wing shape for a small jet aircraft using kriging model. *44th AIAA Aerospace Sciences Meeting*, Reno, NV. pp. 11158-11170.

Kumano, T., Jeong, S., Obayashi, S., Ito, Y., Hatanaka, K., and Morino, H. (2006b). Multidisciplinary design optimization of wing shape with nacelle and pylon. *European Conference on Computational Fluid Dynamics (ECCOMAS CFD 2006)*, Egmond aan Zee, The Netherlands.

Kumano, T., Morino, H., Jeong, S., and S., O. (2008). Aeroelastic analysis using unstructured CFD method for realistic aircraft design. *8th World Congress on Computational Mechanics / 5th European Congress on Computational Methods in Applied Sciences and Engineering*, Venice, Italy.

Ligetti, C. B. and Simpson, T. W. (2005). Metamodel-driven design optimization using integrative graphical design interfaces: Results from a job-shop manufacturing simulation experiment. *Journal of Computing and Information Science in Engineering*, 5, 8-17.

Ligetti, C., Simpson, T. W., Frecker, M., Barton, R. R., and Stump, G. (2003). Assessing the impact of graphical design interfaces on design efficiency and effectiveness. *Journal of Computing and Information Science in Engineering*, 3, 144-154.

Makino, Y. and Naka, Y. (2007). Sonic-boom research and low-boom demonstrator project in JAXA. *Proceedings on 19th International Congress on Acoustics*, Madrid, Spain.

Mattson, C. A. and Messac, A. (2003). Concept selection using s-pareto frontiers. *AIAA Journal*, 41, 1190-1198.

McKay, M. D., Beckman, R. J., and Conover, W. J. (1979). A comparison of three methods for selecting values of input variables in the analysis of output from a computer code. *Technometrics*, 21, 239-245.

Messac, A. and Chen, X. (2000). Visualizing the optimization process in real-time using physical programming. *Engineering Optimization*, 32, 721-747.

Morino, H., Yamaguchi, H., Kumano, T., Jeong, S., and Obayashi, S. (2009). Efficient aeroelastic analysis using unstructured CFD method and reduced-order unsteady aerodynamic model. *50th AIAA/ASME/ASCE/AHS/ASC Structures, Structural Dynamics, and Materials Conference*, Palm Springs, CA. pp. AIAA 2009-2326.

Murakami, A. (2006). Silent supersonic technology demonstration program. *Proceedings on 25th International Council of the Aeronautical Sciences*, Hamburg, Germany.

Obayashi, S., Jeong, S., and Chiba, K. (2005). Multi-objective design exploration for aerodynamic configurations. *35th AIAA Fluid Dynamics Conference and Exhibit*. pp. AIAA-2005-4666.

Obayashi, S., Jeong, S., Chiba, K., and Morino, H. (2007). Multi-objective design exploration and its application to regional-jet wing design. *Transactions of The Japan Society for Aeronautical and Space Sciences*, 50, 1-8.

Obayashi, S. and Sasaki, D. (2003). Visualization and data mining of Pareto solutions using self-organizing map. *2nd International Conference on Evolutionary Multi-Criterion Optimization*, Faro, Portugal. pp. 796-809.

Ohnuki, T., Hirako, K., and Sakata, K. (2006). National experimental supersonic transport project. *Proceedings on 25th International Council of the Aeronautical Sciences*, Hamburg, Germany.

Ohrn, A. (2000). *ROSETTA Technical Reference Manual*. Trondheim, Norway: Department of Computer and Information Science, Norwegian University of Science and Technology.

Oyama, A., Verburg, P. C., Nonomura, T., Hoeijmakers, H. W. M., and Fujii, K. (2010). Flow field data mining of Pareto-optimal airfoils using proper orthogonal decomposition. *48th AIAA Aerospace Sciences Meeting Including the New Horizons Forum and Aerospace Exposition*, Orlando, FL. pp. AIAA 2010-1140.

Parashar, S., Pediroda, V., and Poloni, C. (2008). Self organizing maps (SOM) for design selection in robust multi-objective design of aerofoil. *46th AIAA Aerospace Sciences Meeting and Exhibit*, Reno, NV.

Parker, S. G., Weinstein, D. M., and Johnson, C. R. (1997). The SCIRun computational steering software system. In E. Arge, A. M. Bruaset, and H. P. Langtangen, eds. *Modern Software Tools for Scientific Computing*. Boston: Birkhauser. p. 380 p.

Pawlak, Z. (1982). Rough sets. *International Journal of Computer & Information Sciences*, 11, 341-356.

Paxson, D. E. and Skoch, G. J. (1998). Wave augmented diffusers for centrifugal compressors. *34th AIAA/ASME/SAE/ASEE Joint Propulsion Conference and Exhibit*, Reston, VA. pp. AIAA 98-3401.

Pohlheim, H. (1999). Visualization of evolutionary algorithms: set of standard techniques and multidimensional visualization. *Genetic and Evolutionary Computation Conference*, San Francisco, CA. pp. 533-540.

Pryke, A., Mostaghim, S., and Nazemi, A. (2007). Heatmap visualization of population based multi objective algorithms. *4th International Conference on Evolutionary Multi-Criterion Optimization*, Matsushima, Japan. pp. 361-375.

Queipo, N. V., Haftka, R. T., Shyy, W., Goel, T., Vaidyanathan, R., and Kevin Tucker, P. (2005). Surrogate-based analysis and optimization. *Progress in Aerospace Sciences*, 41, 1-28.

Shimoyama, K., Sugimura, K., Jeong, S., and Obayashi, S. (2010). Performance map construction for a centrifugal diffuser with data mining techniques. *Journal of Computational Science and Technology*, 4, 36-50.

Simon, H., Wallmann, T., and Moenk, T. (1987). Improvements in performance characteristics of single-stage and multistage centrifugal compressors by simultaneous adjustments of inlet guide vanes and diffuser vanes. *Journal of Turbomachinery*, 109, 41-47.

Simpson, T. W., Carlsen, D. E., Congdon, C. D., Stump, G., and Yukish, M. A. (2008). Trade space exploration of a wing design problem using visual steering and multi-dimensional data visualization. *49th AIAA/ASME/ASCE/AHS/ASC Structures, Structural Dynamics, and Materials Conference*, Schaumburg, IL. pp. AIAA 2008-2139.

Simpson, T. W., Iyer, P. S., Rothrock, L., Frecker, M., Barton, R. R., Barron, K. A., and Meckesheimer, M. (2005). Metamodel-driven interfaces for engineering design: Impact of delay and problem size on user performance. *46th AIAA/ASME/ASCE/AHS/ASC Structures, Structural Dynamics and Materials Conference*, Austin, TX. pp. 3198-3208.

Sobol, I. M. (1993). Sensitivity estimates for nonlinear mathematical models. *Mathematical Modeling and Computational Experiments*, 1, 407-414.

Stump, G., Lego, S., Yukish, M., Simpson, T. W., and Donndelinger, J. A. (2009). Visual steering commands for trade space exploration: User-guided sampling with

example. *Journal of Computing and Information Science in Engineering*, 9, 1-10.

Stump, G., Simpson, T. W., Yukish, M., and Bennett, L. (2002). Multidimensional visualization and its application to a design by shopping paradigm. *9th AIAA/ISSMO Symposium on Multidisciplinary Analysis and Optimization*, Atlanta, GA. pp. AIAA 2002-5622.

Stump, G. M., Simpson, T. W., Yukish, M., and O'Hara, J. J. (2004). Trade space exploration of satellite datasets using a design by shopping paradigm. *IEEE Aerospace Conference Proceedings*, Big Sky, MT. pp. 3885-3894.

Sugimura, K., Jeong, S., Obayashi, S., and Kimura, T. (2009a). Kriging-model-based multi-objective robust optimization and trade-off rule mining of a centrifugal fan with dimensional uncertainty. *Journal of Computational Science and Technology*, 3, 196-211.

Sugimura, K., Obayashi, S., and Jeong, S. (2009b). A new design method based on cooperative data mining from multi-objective design space. *Journal of Computational Science and Technology*, 3, 287-302.

Sugimura, K., Obayashi, S., and Jeong, S. (2010). Multi-objective optimization and design rule mining for an aerodynamically efficient and stable centrifugal impeller with a vaned diffuser. *Engineering Optimization*, 42, 271-293.

Svensen, M. (1998). *GTM: The Generative Topographic Mapping*. PhD Thesis, Aston University.

Takenaka, K., Hatanaka, K., Yamazaki, W., and Nakahashi, K. (2008). Multidisciplinary design exploration for a winglet. *Journal of Aircraft*, 45, 1601-1611.

Takenaka, K., Obayashi, S., Nakahashi, K., and Matsushima, K. (2005). The application of MDO technologies to the design of a high performance small jet aircraft-lessons learned and some practical concerns. *35th AIAA Fluid Dynamics Conference and Exhibit*, Toronto, Ontario. pp. AIAA 2005-4797.

van Wijk, J. J. and Liere, R. V. (1993). HyperSlice: visualization of scalar functions of many variables. *IEEE Visualization Conference*, San Jose, CA. pp. 119-125.

Winer, E. H. and Bloebaum, C. L. (2002a). Development of visual design steering as an aid in large-scale multidisciplinary design optimization. Part I: Method development. *Structural and Multidisciplinary Optimization*, 23, 412-424.

Winer, E. H. and Bloebaum, C. L. (2002b). Development of visual design steering as an aid in large-scale multidisciplinary design optimization. Part II: Method validation. *Structural and Multidisciplinary Optimization*, 23, 425-435.

Witten, I. H. and Frank, E. (2005). *Data Mining: Practical Machine Learning Tools and Techniques*. 2nd ed. Boston: Morgan Kaufman.

Wong, P. C. and Bergeron, R. D. (1997). 30 years of multidimensional multivariate visualization. *Proceeding Scientific Visualization, Overviews, Methodologies, and Techniques*. pp. 2-33.